Published in Applied Optics ***41****(25), 5405-5412 (2002)*

Polarized light scattering by dielectric and metallic spheres on silicon wafers

Jung Hyeun Kim,[a,b] Sheryl H. Ehrman,[b] George W. Mulholland,[c] and Thomas A. Germer[a]
[a]*Optical Technology Division, National Institute of Standards and Technology, Gaithersburg, MD 20899*
[b]*Department of Chemical Engineering, University of Maryland, College Park, MD 20742*
[c]*Fire Research Division, National Institute of Standards and Technology, Gaithersburg, MD 20899*

Abstract: The polarization and intensity of light scattered by monodisperse polystyrene latex (PSL) and copper spheres, having diameters ranging from 92 nm to 218 nm, deposited on silicon substrates were measured using 442 nm, 532 nm, and 633 nm light. The results are compared to a theory for scattering by a sphere on a surface, originally developed by Bobbert and Vlieger, and extended to include coatings on the sphere and the substrate. The results show that accurate calculation of the scattering of light by a metal sphere requires that the near-field interaction between the sphere and its image be included in a complete manner. The normal incidence approximation does not suffice for this interaction, and the existence of any thin oxide layer on the substrate must be included in the calculation.

OCIS codes: 240.0240, 290.0290, 350.4990, 120.5820

1. Introduction

Light scattering is used by the semiconductor, optical, and data storage industries to inspect materials for surface quality.[1] The development of more sensitive and accurate light scattering tools requires understanding the scattering behavior of the different types of defects that the tools are expected to encounter. Theoretical models, validated by well-characterized measurements, enable manufacturers to predict and optimize the performance of their tools. While numerous studies have investigated the scattering of light by small dielectric spheres,[2–7] and while such spheres are often used for calibrating scanning surface inspection systems, the scattering from such spheres does not necessarily behave like that from real production line particle defects. Furthermore, the scattering by metallic particles is complicated by the much stronger near-field interaction between the particle and the substrate, requiring a model which treats this near-field interaction completely. The development and validation of a robust scattering theory for a sphere on a substrate creates a benchmark by which approximate codes for arbitrarily-shaped structures can be tested.[4,8]

Several studies have shown that the polarization of scattered light can be used to characterize and distinguish among different types of defects, such as particulate contaminants,[9] surface roughness,[10,11] and subsurface defects.[9,10] In this paper, we present measurements and theoretical calculations for light scattering from polystyrene latex (PSL) and copper spheres deposited on silicon surfaces. The polarization state and the differential scattering cross section for light scattering from particles having diameters ranging from 92 nm to 218 nm have been measured as functions of incident angle and scattering angle, using polarized, visible laser light. Theoretical calculations, based on the theory of Bobbert and Vlieger[12] (BV),

are compared to the data. By comparing the BV theory to approximate models, namely Nahm and Wolfe's Mie-Surface Double Interaction model[2] (MSDI) and Videen's Normal Incidence Approximation[13,14] (NIA), we gain insight on how different aspects of the scattering are controlled by different parameters of the particles. As expected, metal particles show a more complicated interaction with the silicon substrate than do dielectric particles.

We briefly describe the theory of Bobbert and Vlieger in Sec. 2. In Sec. 3, we describe our preparation of samples containing size-monodisperse PSL or copper spheres deposited onto silicon surfaces. We then describe in Sec. 4 polarized light scattering measurements that we performed on those samples. We present and discuss the results of theoretical calculations and the light scattering measurements in Sec. 5. Finally, we summarize our findings in Sec. 6.

2. Theory

Figure 1 describes the geometry of a particle above a substrate. A sphere of refractive index n_2 and radius r lies a distance δ above an interface. The substrate of refractive index n_0 has a coating of refractive index n_1 and thickness t. Bobbert and Vlieger (BV) published a solution to the scattering of light by such a sphere on a substrate in 1986.[12] To solve this problem, space is divided into three regions: Σ_1, a spherical region containing the particle, Σ_2, a spherical shell outside of the particle and containing only free space, and Σ_3, all of the space, including the substrate, outside of Σ_2 and Σ_1. Fields in Σ_3 are most naturally represented using a plane-wave basis, with the interface being accounted for by the Fresnel reflection coefficients appropriate for a single coating layer.

Fields in Σ_1 and Σ_2 are best represented using vector spherical harmonics or spherical Debye potentials. The Mie scattering solution for a free-space sphere applies to regions Σ_1 and Σ_2 and provides the relationship between the inward propagating fields and the outward propagating fields represented with vector spherical harmonics or spherical Debye potentials. BV derived the spherical Debye potential form of the surface reflection matrix, thereby relating the inward and outward propagating fields in Σ_2. By self-consistently including the reflection of the surface into the Mie scattering solution, the solution to the fields in Σ_2 can be found. It is then straightforward to solve for the fields in Σ_1 and Σ_3. The solution for a sphere bound to a substrate is obtained from the limit $\delta \to 0$.

Bobbert, Vlieger, and Greef[15] (BVG) presented numerical methods to evaluate the BV theory, and applied it to mercury spheres above a graphite substrate in an aqueous surrounding. In practice, one must truncate the field expansions, allowing the spherical harmonic order l to vary from 1 to a specified l_m. Convergence of the solution is most rapid when either the surface or the sphere has a relative index near unity. Since the relative complex refractive index of the spheres (Hg) compared to the surrounding (H_2O) was $1.44 + 4.11i$, while that of the substrate (graphite) was $1.47 + 0.60i$, convergence was rapid. In contrast, the solution for a noble metal sphere, such as copper, on a high-index substrate, such as silicon, in an ambient air environment does not converge rapidly. In such cases, since the solution requires the matching of high-order spherical harmonics on the interfaces, the scattering function is expected to be very sensitive to the shape of the particle.[16]

The substrate reflection matrix is given by BV with respect to the reflection coefficients of the substrate, $r_s(\theta)$ and $r_p(\theta)$, as integrals over complex angles θ. When the substrate is coated with a material of index n_1 and thickness t, the reflection coefficients are given by

$$r_k(\theta) = [\tilde{r}_k(\theta,1,n_1) + \tilde{r}_k(\theta,n_1,n_2)\,\mathrm{e}^{2\mathrm{i}q(\theta)t}]/[1 + \tilde{r}_k(\theta,1,n_1)\tilde{r}_k(\theta,n_1,n_2)\,\mathrm{e}^{2\mathrm{i}q(\theta)t}] \tag{1}$$

(k = s,p) where

$$\tilde{r}_s(\theta,N_1,N_2) = [(N_1^{\,2} - \sin^2\theta)^{1/2} - (N_2^{\,2} - \sin^2\theta)^{1/2}]/ [(N_1^{\,2} - \sin^2\theta)^{1/2} + (N_2^{\,2} - \sin^2\theta)^{1/2}] \tag{2a}$$

$$\tilde{r}_p(\theta,N_1,N_2) = [N_2^{\,2}(N_1^{\,2} - \sin^2\theta)^{1/2} - N_1^{\,2}(N_2^{\,2} - \sin^2\theta)^{1/2}]/ [N_2^{\,2}(N_1^{\,2} - \sin^2\theta)^{1/2} + N_1^{\,2}(N_2^{\,2} - \sin^2\theta)^{1/2}] \tag{2b}$$

$$q(\theta) = 2\pi(n_1^{\,2} - \sin^2\theta)^{1/2}/\lambda\,. \tag{3}$$

The presence of a low index coating on the substrate serves to reduce the reflectance, especially for large complex angle θ, and thus substantially increases the rate of convergence.

While the BV theory was initially applied to a homogeneous spherical particle, it is straightforward to extend the theory to include coatings on the particle. The presence of a coating on the sphere can be incorporated into the BV theory by replacing the formula for the Mie scattering matrix B by an appropriate matrix for a coated sphere, such as that given by Sec. 8.1 of Ref. 17. The BV theory can be further extended to treat non-spherical particles using the T-matrix method.[18–20] We forego discussion of these extensions and their results to other publications.[16]

Following the steps outlined by BVG, we can calculate the scattering function to an arbitrary level of accuracy. Our implementation of the code has been written in C++, and has been included in a library of scattering models available on the Internet.[21] The computation time on a modern desktop computer is about 10 s for $l_{\mathrm{m}} = 30$ and scales as approximately $l_{\mathrm{m}}^{3.4}$. Two approximations that have been used in the past are the Mie-surface double interaction (MSDI) model of Nahm and Wolfe[2] and the normal incidence approximation (NIA) of Videen.[13,14] The MSDI model can be evaluated using the BV theory by ignoring the interaction of the sphere with its image in the substrate, that is, by making the approximation that the near-field reflection matrix A = 0. The NIA model can be evaluated by letting the reflection coefficients be given by their normal incidence values $r_k(\theta) = r_k(0)$ during the evaluation of the matrix A. In Sec. 5, we will use these approximations to demonstrate the importance of the near field interaction of the particle with the surface.

3. Sample Preparation

We prepared samples containing size-monodisperse spheres of PSL and copper deposited onto silicon wafers. In this section, we describe the techniques that we employed to produce those samples and to perform the deposition.

A. PSL spheres

PSL spheres suspended in de-ionized water were atomized into aerosol droplets using a nebulizer. The aerosol stream containing PSL spheres flows through a bipolar charger where particles are charged

with a Boltzmann charge distribution. The aerosol stream flows through a cylindrical electrostatic differential mobility analyzer (DMA), where the spheres experience an electrostatic force and a viscous drag force and move radially from an entrance slit at the outside of the analyzer to an exit slit on an inner cylinder. Given specific voltage and flow conditions, a characteristic size of particles is classified. In order to have a minimum number of doublet spheres, original PSL suspension of 5 % mass concentration was diluted by adding one drop to 2000 mL of deionized and filtered water (0.2 μm pore size) before being nebulized. The concentration of the PSL spheres was low enough that the fraction of droplets containing multiple spheres was less than 0.01. Thus, most droplets containing PSL spheres evaporate leaving a single sphere. While it is possible that doubly charged doublet PSL particles reach the sample, the use of a DMA prevents any significant number of solvent residue particles from reaching the sample. Details of DMA size classification are described elsewhere.[22] We deposited three different sizes of PSL spheres: 101 nm, 155 nm, and 218 nm.

B. Copper spheres

Copper spheres were generated before being deposited onto wafers. Solution droplets containing copper nitrate were generated by nebulization using compressed nitrogen, and the droplets were carried by nitrogen gas into a high temperature furnace (1000 °C). The solvent evaporated and the copper nitrate residue particles decomposed in the presence of the vaporized solvent to produce pure copper spherical particles. Transmission electron microscopy (TEM) verified that the copper particles were spherical with cross sectional diameters differing from the mean diameter by at most 10 %.[23] The particles were size-classified from the polydisperse aerosol using a bipolar charger and a DMA operated at specific applied voltage and flow conditions to yield spheres of diameters 92 nm, 123 nm, and 155 nm. We used the NIST 100.7 nm PSL sphere Standard Reference Material (SRM® 1963),[24] to calibrate the DMA for the modal diameter of copper spheres. In addition, the classified particle sizes were verified by TEM. The details of the pure copper formation and classification are described elsewhere.[23] The process used to create the copper particles and the use of a DMA to classify them prevents any significant number of doublets or solvent residue particles from reaching the sample.

C. Particle deposition

An electrostatic precipitator (ESP) connected to the particle generation and classification system was used to deposit spheres onto clean silicon wafers. The spheres, which remain charged after being size-classified, are subject to an electric field (5000 V/cm) between the aerosol stream inlet and the wafer.[24] We used a dark field optical microscope to count the deposited particles to determine the particle number density. The particle number density was obtained by averaging particle counts from 50 to 100 locations. The uncertainties in the modal diameter, the estimated full width at half maximum (FWHM) of the diameter distribution, and the particle number densities ρ are shown in Table 1. We had difficulty measuring the number density for the 101 nm PSL spheres by optical microscopy due to their low scattering intensity. Prior to depositing any particles, all wafers (diameter 25.4 mm) were cleaned with the RCA cleaning procedure[25] and checked by light scattering. The bidirectional reflectance distribution function (BRDF) from a clean wafer was about 4×10^{-8} sr^{-1} at the wavelength λ = 633 nm for typical non-specular geometries. The indices of refraction of PSL, copper, silicon, and silicon dioxide for the model

calculations are shown in Table 2. All cleaned wafers were assumed to have an approximately 1.5 nm thick native oxide layer, typical for wafers exposed to air.[26]

4. Optical Scattering Measurements

Samples were produced having a surface density ρ of size-monodisperse spheres. Linearly polarized light of wavelength λ was incident upon each sample at an angle θ_i. Light scattered into a direction defined by polar angle θ_r and azimuthal angle ϕ_r was detected, yielding a differential scattering cross section, and analyzed for polarization state. A goniometric optical scatter instrument, described elsewhere,[27,28] was used to perform the measurements. We used three laser sources to produce three wavelengths: λ = 442 nm (HeCd), 532 nm (Nd:YAG), and 633 nm (HeNe). The laser beam at the sample was approximately 1 mm in diameter. Specific incident polarizations were chosen to yield high differentiation amongst different particle sizes. While measurements were performed both in the plane of incidence and out of the plane of incidence, we show only results in the plane of incidence. In-plane measurements using 45° incident polarization are presented for a fixed incident angle θ_i = 60°, scanning the viewing angle θ_r. In all measurements, the scattered light was analyzed for polarization state using a rotating-compensator-fixed-polarizer arrangement. The differential scattering cross section is given by

$$\frac{d\sigma}{d\Omega} = \frac{d\Phi_r}{d\Omega}\frac{\cos\theta_i}{\Phi_i \rho}, \tag{4}$$

where Φ_i and $d\Phi_r$ are the incident and scattered power, respectively, and $d\Omega$ is the collection solid angle. The differential scattering cross section relates the intensity on a single particle to the power scattered by it per solid angle.

The polarization state of the light is parameterized by its principal angle of polarization η, its degree of circular polarization P_C, and its total degree of polarization P. The angle η is measured from s-polarization in a right-handed fashion (counterclockwise, looking into the beam). The value of P_C is positive for left-circularly polarized light. Since some depolarization was observed in the data, we show the normalized degree of circular polarization P_C/P. The normalized value is more appropriate to compare to theory, since all of the theories predict P = 1. While a complete uncertainty analysis has not been performed for these measurements, the uncertainties in $d\sigma/d\Omega$, η, P_C, and P are expected to be dominated by statistical sources and can be estimated by observing the point-to-point variation in the data.

5. Results and Discussion

Figures 2 and 3 show comparisons of the MSDI model, NIA model, and the BV theory for 155 nm PSL and copper spheres, respectively, on a silicon wafer using λ = 633 nm. The three theories predict similar behaviors for the PSL sphere (Fig. 2), indicating that the near-field interaction between the sphere and the substrate, which is ignored in the MSDI model and incompletely treated in the NIA model, is weak. In comparison, the three theories predict very different results for copper spheres (Fig. 3), where the sphere-surface interaction is much stronger. The NIA model, for example, predicts a differential scattering cross section differing by as much as a factor of three from the BV theory at some scattering angles. The failure of the NIA model further suggests that large surface wavevectors (large complex angle) contribute to the near-field interaction. This finding is consistent with the very slow convergence of the BV theory for

copper, requiring values of l_m on the order of 30 to 60, compared to 7 to 10 for PSL. The slow convergence also suggests that the scattering will be very sensitive to the shape of the particle.[16] The use of the full BV theory is clearly necessary when comparing data to theoretical calculations. While the scattering by PSL spheres is relatively independent of scattering model, the BV theory must still be used when using light scattering to accurately size them.

The scattering from metal spheres on a surface depends strongly on the existence and thickness of any dielectric layer on the substrate. Figures 4 and 5 show comparisons of the BV theory for scattering from 155 nm PSL and copper spheres, respectively, on thin SiO_2 layers on the substrate at $\lambda = 633$ nm, with thicknesses ranging from $t = 0.5$ nm to 2.5 nm. These oxide layers are thin enough that they are nearly imperceptible to any far field reflectance measurement. The scattering by PSL spheres (Fig. 4) is relatively unperturbed by the existence of such a layer. However, the effects of the layer are significant for the copper spheres (Fig. 5), with $d\sigma/d\Omega$ changing by more than a factor of two at some angles and the polarization state being significantly perturbed. The implications of this strong thickness dependence are interesting. Near-field scattering probes are the subject of a great deal of current literature and rely upon this sensitivity to obtain sub-wavelength optical characterization of surface features.[30,31] When using metallic spheres as a scattering standard, however, the sensitivity to substrate film thickness may pose a problem: the scattering from metallic spheres may depend too strongly on the condition of the substrate to reliably provide a stable scattering source. In all of the theory-experiment comparisons that follow, the existence of a 1.5 nm native oxide layer on the silicon substrate is included in the calculations.

In-plane and out-of-plane measurements, carried out for a variety of incident and scattering directions and polarization conditions, produced excellent agreement with the BV predictions. However, for simplicity, we demonstrate the agreement here with only the in-plane measurements and with $\theta_i = 60°$. Figures 6 and 7 show the light scattering parameters measured in the plane of incidence using 45°-polarized light of wavelength $\lambda = 442$ nm for the PSL and copper spheres, respectively. In all of the data, a marked increase in the measured differential cross section and deviations in the polarization state occur near the specular direction at $\theta_r = 60°$. Near this direction, the scatter is dominated by surface roughness and flatness rather than the particles. Data are also excluded from a small region near $\theta_r = -60°$, where the detector assembly obscures the incident laser beam. For the remaining data, the measurements for both dielectric PSL spheres and metallic copper spheres show excellent agreement with the BV theory. The $d\sigma/d\Omega$ for 101 nm PSL spheres shows some differences from the BV predictions. However, the 101 nm PSL sphere data parallels the BV theory, suggesting that the density, a constant factor in the calculation of $d\sigma/d\Omega$ (see Eq. 4), was incorrect. As we mentioned above in Sec. 3.C., we attribute this constant factor to our poor ability to measure the surface number density of the 101 nm PSL spheres.

In addition to the measurements with varying sphere sizes, we performed measurements with different wavelengths to assure us that the BV theory is applicable over a wide range of experimental variables. As can be seen from Table 2, the optical properties of copper vary by a large amount between 442 nm and 633 nm. Thus, measuring the wavelength dependence of the scattering is tantamount to extending the measurements to other materials. Figures 8 and 9 show the scattering parameters measured in the plane of incidence with 45°-polarized light using the three wavelengths ($\lambda = 442$ nm, $\lambda = 532$ nm, and $\lambda = 633$ nm) for the 155 nm PSL and copper spheres, respectively, at $\theta_i = 60°$. The agreement between the measured principal polarization angles η and the normalized degree of circular polarization P_c/P and those predicted by the BV theory is very good. The data presented in Fig. 9 for copper spheres at 633 nm, for which the BV theory was compared to the MSDI and NIA models in Fig. 3, demonstrates that the full BV theory must be used for metallic particles. As above, some deviations can be seen in the $d\sigma/d\Omega$. The

data lie parallel to the theory, suggesting an error in a constant multiplicative value. Since the densities should be constant for a specific sample, we do not understand shy the multiplicative factor changes with wavelength. It may be a result of an unknown instrumental artifact or variations of the density across the sample surface.

For a dilute, non-interacting, size-monodisperse collection of spheres on a surface we would not expect to observe any depolarization. However, the measurements presented in Figs. 6–9 show some depolarization ($P < 1$), especially at large scattering angles. The depolarization may result from the finite width of the particle-size distributions (see Table 1), non-sphericity of the particles, multiple scattering from particles, or interference from other scattering sources. We estimated the effect of the finite width of the particle size, by performing an integral of the Stokes vector over particle diameter, and found the degree of polarization to remain above 0.99 for all of the particles. Calculations of scattering by slightly non-spherical dielectric and metallic spheres suggest that the scattering by PSL spheres is relatively insensitive to particle shape, while that by copper spheres is very sensitive to shape.[16] However, the amount of observed depolarization is similar for both particle materials, suggesting that variations from spherical shape do not account for the observed depolarization. The high particle densities may lead to multiple scattering from particles. However, even on the highest density samples, the mean distance between particles ($\rho^{-1/2}$) is approximately 100 times the particle diameter. Therefore, since the substrate does not support guided waves, multiple scattering should not contribute significantly to the scatter.

Scattering from residual roughness of the samples, or from foreign particles, could contribute considerably to the scatter. Before particle deposition, the wafers had scattering levels only an order of magnitude below that of the minimum signal observed with the particles. Furthermore, foreign particles cannot be ruled out, as it was found that certain areas of each wafer were found to have considerably higher scattering levels and were consequently avoided. Since the depositions covered most of the wafer surface, no effort was made to perform measurements that could be used to subtract the background scattering level.

6. Conclusion

The scattering of polarized light by PSL and copper spheres on silicon surfaces was measured for a variety of sphere diameters and wavelengths. By using wavelengths across the visible spectrum for the copper spheres, in addition to those for the PSL spheres, we have obtained results for a relatively wide range of particle optical properties. The results agree well with the predictions of the BV theory for a sphere on a substrate, provided we include the presence of the thin oxide layer on the substrate. The agreement with this theory establishes the accuracy of the BV model, providing a benchmark for other approximate theories. Comparisons of the BV theory with two approximate theories demonstrate the need to properly account for the near-field interaction between the sphere and its image in the substrate. The results presented here provide the foundation necessary to enable light scattering to be used as a method for determining diameter of surface-bound particles.

References

1. J. C. Stover, *Optical Scattering: Measurement and Analysis*, (SPIE Optical Engineering Press, Bellingham, WA, 1995).
2. K. B. Nahm and W. L. Wolfe, "Light-scattering models for spheres on a conducting plane: comparison with experiment," Appl. Opt. **26,** 2995–2999 (1987).
3. P. R. Spyak and W. L. Wolfe, "Scatter from particulate-contaminated mirrors. Part 1: theory and experiment for polystyrene spheres and λ=0.6328 μm," Opt. Eng. **31,** 1746–1756 (1992).
4. G. W. Starr and E. D. Hirleman, "Comparison of Experimentally Measured Differential Scattering Cross Sections of PSL Spheres on Flat Surfaces and Patterned Surfaces," in *Flatness, Roughness, and Discrete Defect Characterization for Computer Disks, Wafers, and Flat Panel Displays,* J. C. Stover, Ed., Proc. SPIE, **2862**, 130–138 (1996).
5. L. Sung, G. W. Mulholland, and T. A. Germer, "Polarized light-scattering measurements of dielectric spheres upon a silicon surface," Opt. Lett. **24,** 866–868 (1999).
6. Y. A. Eremin, J. C. Stover, and N. V. Orlov, "Modeling scatter from silicon wafer features based on discrete sources method," Opt. Eng. **38,** 1296–1304 (1999).
7. D. C. Weber and E. D. Hirleman, "Light scattering signatures of individual spheres on optically smooth conducting surfaces," Appl. Opt. **27,** 4019–4026 (1988).
8. R. Schmehl, B. M. Nebeker, and E. D. Hirleman, "Discrete-dipole approximation for scattering by features on surfaces by means of a two-dimensional fast Fourier transform technique," J. Opt. Soc. Am. A **14,** 3026–3036 (1997).
9. T. A. Germer, "Angular dependence and polarization of out-of-plane optical scattering from particulate contamination, subsurface defects, and surface microroughness," Appl. Opt. **36,** 8798–8805 (1997).
10. T. A. Germer and C. C. Asmail, "Polarization of light scattered by microrough surfaces and subsurface defects," J. Opt. Soc. Am. A **16,** 1326–1332 (1999).
11. T. A. Germer, C. C. Asmail, and B. W. Scheer, "Polarization of out-of-plane scattering from microrough silicon," Opt. Lett. **22,** 1284–1286 (1997).
12. P. A. Bobbert and J. Vlieger, "Light scattering by a sphere on a substrate," Physica **137A,** 209–242 (1986).
13. G. Videen, "Light scattering from a sphere on or near a surface," J. Opt. Soc. Am. A **8,** 483–489 (1991).
14. G. Videen, "Light scattering from a sphere on or near a surface: errata," J. Opt. Soc. Am. A **9,** 844–845 (1992).
15. P. A. Bobbert, J. Vlieger, and R. Greef, "Light reflection from a substrate sparsely seeded with spheres—comparison with an ellipsometric experiment," Physica **137A,** 243–257 (1986).
16. T.A. Germer, "Light scattering by slightly non-spherical particles on surfaces," Opt. Lett. in press (July 1, 2002).

C. F. Bohren and D. R. Huffman, *Absorption and Scattering of Light by Small Particles*, (Wiley, New York, 1983).

T. Wriedt and A. Doicu, "Light scattering from a particle on or near a surface," Opt. Commun. **152**, 376–384 (1998).

A. Doicu, Yu. Eremin, and T. Wriedt, "Non-axisymmetric models for light scattering from a particle on or near a plane surface," Opt. Commun. **182**, 281–288 (2000).

20. G. Videen, "Light scattering from a particle on or near a perfectly conducting surface," Opt. Commun. **115**, 1–7 (1995).
21. T. A. Germer, *SCATMECH: Polarized Light Scattering C++ Class Library* (available at http://physics.nist.gov/scatmech, 2000).

22. P. D. Kinney, D. Y. H. Pui, G. W. Mulholland, and N. P. Bryner, "Use of the electrostatic classification method to size 0.1 µm SRM particles—a feasibility study," J. Res. Natl. Inst. Stand. Technol. **96,** 147–176 (1991).
23. J. H. Kim, T. A. Germer, G. W. Mulholland, and S. H. Ehrman, "Size-Monodisperse Metal Nanoparticles via Hydrogen-Free Spray Pyrolysis," Adv. Mater. **14**, 518–521 (2002).
24. G. W. Mulholland, N. P. Bryner, and C. Croarkin, "Measurement of the 100 nm NIST SRM 1963 by Differential Mobility Analysis," Aero. Sci. Tech. **31**, 39–55 (1999).
25. J. Dixkens and H. Fissan, "Development of an Electrostatic Precipitator for Off-Line Particle Analysis," Aero. Sci. Tech. **30,** 438–453 (1999).
26. W. Kern and D. A. Puotinen, "Cleaning solutions based on hydrogen peroxide for use in silicon semiconductor technology," RCA Review **30,** 187–206 (1984).
27. M. Morita, T. Ohmi, E. Hasegawa, M. Kawakami, and M. Ohwada, "Growth of native oxide on a silicon surface," J. Appl. Phys. **68,** 1272–1281 (1990).
28. T. A. Germer and C. C. Asmail, "A goniometric optical scatter instrument for bidirectional reflectance distribution function measurements with out -of-plane and polarimetry capabilities," in *Scattering and Surface Roughness*, Z.-H. Gu and A. A. Maradudin, Eds., Proc. SPIE, **3141**, 220–231 (1997).
29. T. A. Germer and C. C. Asmail, "Goniometric optical scatter instrument for out-of-plane ellipsometry measurements," Rev. Sci. Instr. **70,** 3688–3695 (1999).
30. F. Zenhausern, Y. Martin, and H. K. Wickramasinghe, "Scanning Interferometric Apertureless Microscopy: Optical Imaging at 10 Angstrom Resolution," Science **269,** 1083–1085 (1995).
31. Girard C., Joachim C., and S. Gauthier, "The physics of the near-field," Rep. Prog. Phys. **63,** 893–938 (2000).
32. The uncertainties quoted in this article were obtained by estimating the standard uncertainty σ for the measurement and multiplying by a coverage factor of $k = 2$. These values correspond to a confidence level of 95 %.
33. E. D. Palik, *Handbook of Optical Constants of Solids*, (Academic, San Diego, 1985).
34. R. H. Boundy, R. F. Boyer, and S. M. Stoesser, STYRENE Its Polymers, Copolymers and Derivatives, Chapter 11, pp 523–525 (Reinhold Publishing Corporation, New York, 1952).

Table 1. The modal diameters, distribution widths, and number densities of PSL and copper spheres used in this study.

Spheres	Modal diameter[a] (nm)	Distribution FWHM (nm)	Number density[a] ρ (mm^{-2})
PSL	101 ± 1	5	~ 10000
PSL	155 ± 4[b]	7	3200 ± 170
PSL	218 ± 3	8	380 ± 25
Cu	92 ± 2	5	2800 ± 180
Cu	123 ± 2	7	600 ± 30
Cu	155 ± 3	9	470 ± 30

[a]See Note 32.
[b]Reported from the vendor.

Table 2. Complex indices of refraction for the materials used in the calculations.

Wavelength	Index of refraction			
λ (nm)	Si[a]	SiO_2[a]	Cu[a]	PSL[b]
442	4.76 + 0.17*i*	1.466	1.17 + 2.36*i*	1.615
532	4.15 + 0.05*i*	1.461	1.06 + 2.59*i*	1.598
633	3.88 + 0.02*i*	1.457	0.25 + 3.41*i*	1.588

[a]From Ref. 33.
[b]From Ref. 34.

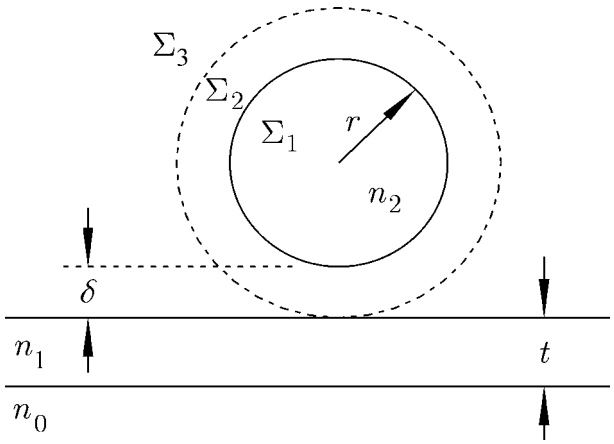

Fig. 1. Schematic of the scattering problem.

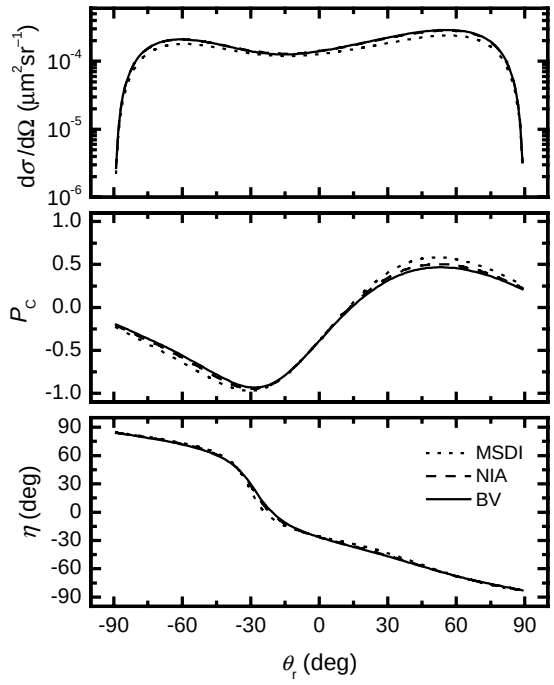

Fig. 2. Light scattering parameters for a 155 nm PSL sphere on a silicon substrate predicted by the MSDI model, NIA model, and the BV theory in the plane of incidence with $\theta_i = 60°$ and $\lambda = 633$ nm. The substrate is assumed to have a 1.5 nm native oxide layer.

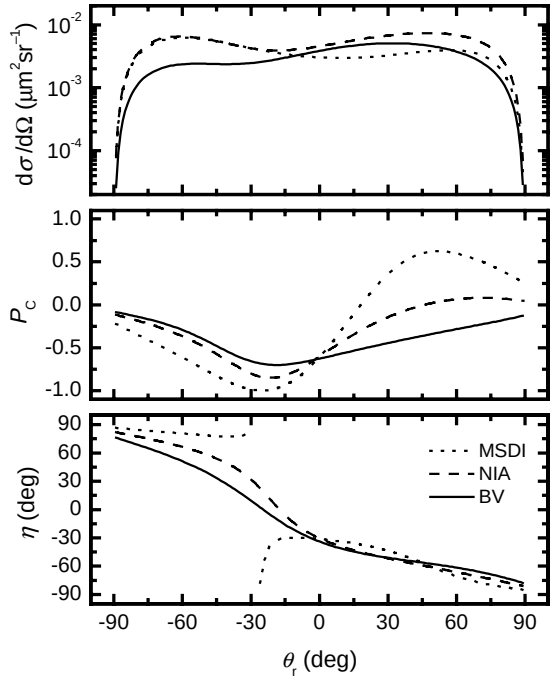

Fig. 3. Same as Fig. 2, except for a 155 nm copper sphere.

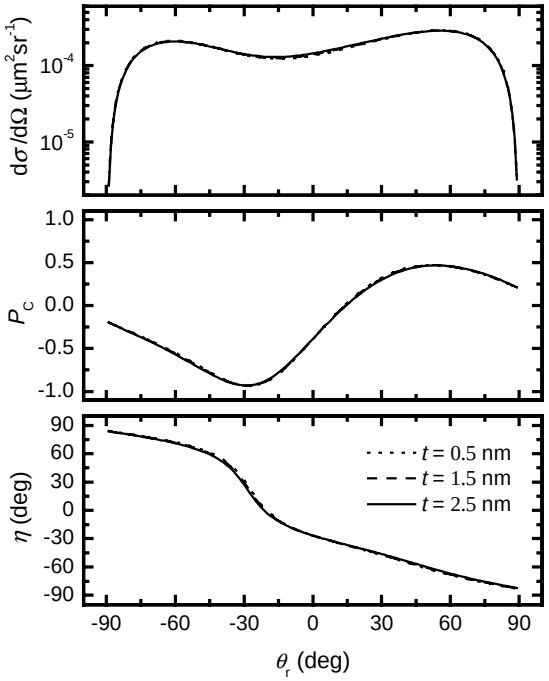

Fig. 4. Light scattering parameters for a 155 nm PSL sphere on a silicon substrate predicted by the BV theory for different SiO_2 layer thicknesses, calculated in the plane of incidence with $\theta_i = 60°$ and $\lambda = 633$ nm.

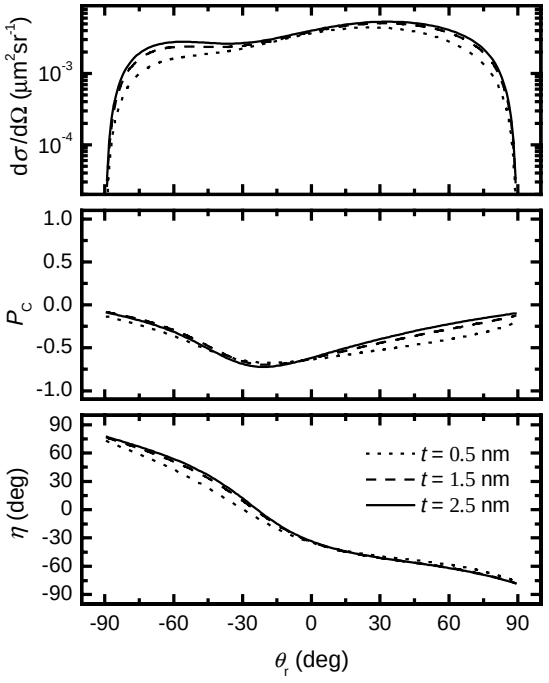

Fig. 5. Same as Fig. 4, except for a 155 nm copper sphere.

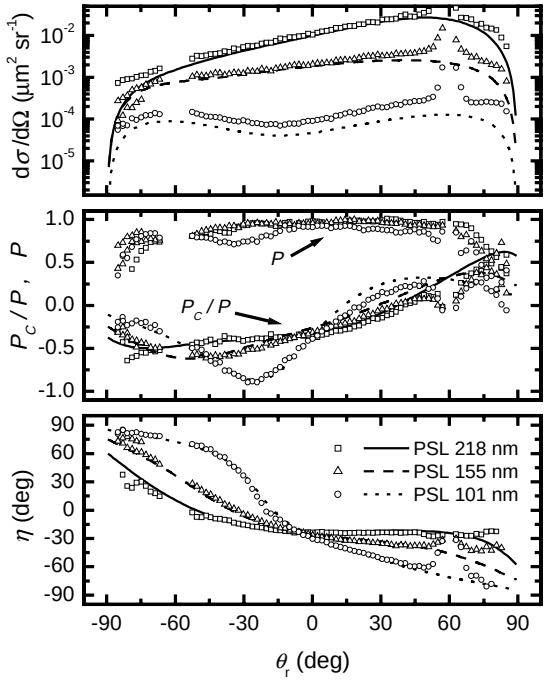

Fig. 6. Light scattering parameters for 101 nm, 155 nm, and 218 nm PSL spheres measured in the plane of incidence with $\theta_i = 60°$ and $\lambda = 442$ nm. The solid curves represent the predictions of the BV theory.

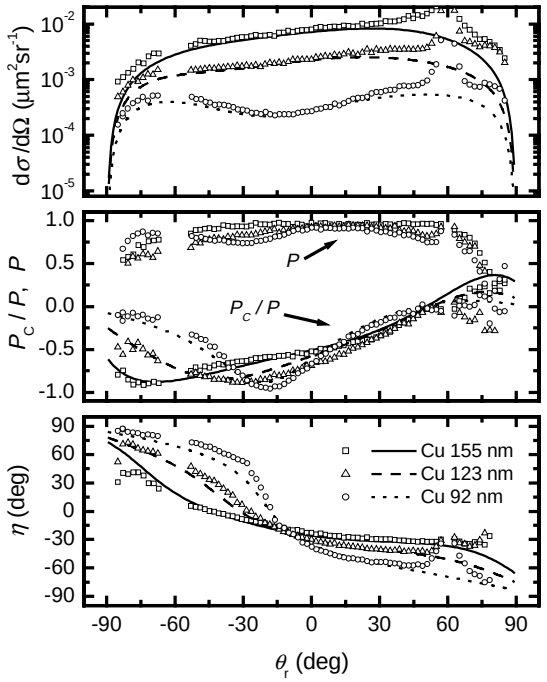

Fig. 7. Same as Fig. 6, except for 92 nm, 123 nm, and 155 nm copper spheres.

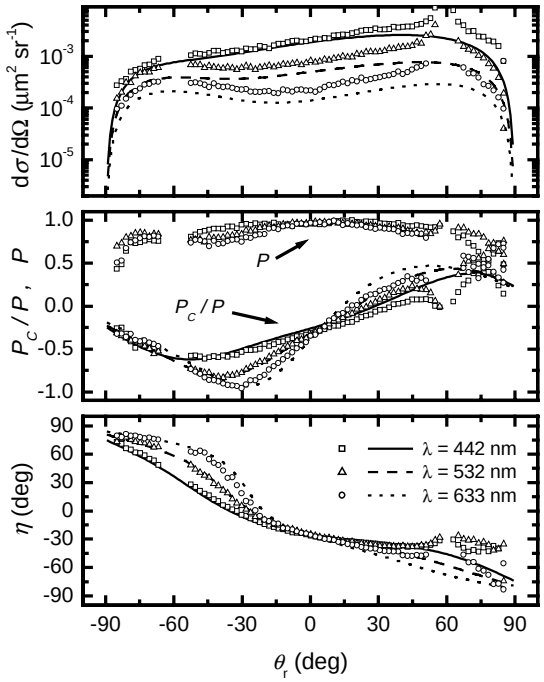

Fig. 8. Light scattering parameters for 155 nm PSL spheres measured in the plane of incidence with $\theta_i = 60°$ using three different wavelengths ($\lambda = 442$ nm, $\lambda = 532$ nm, and $\lambda = 633$ nm). The curves represent the predictions of the BV theory.

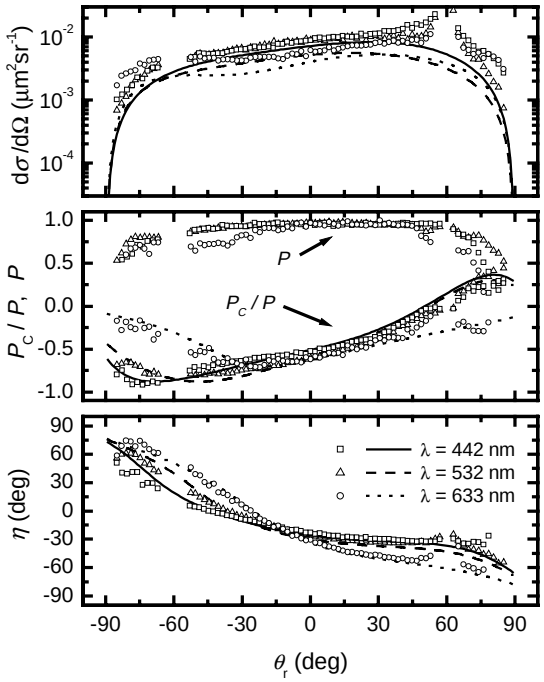

Fig. 9. Same as Fig. 8, except for 155 nm copper spheres.